Electrochemical performance and carbon resistance comparison between Tin, Copper and Silver-Doped Nickel/Yttria-stabilized Zirconia Anodes SOFCs operated with Biogas

Jiang, Zeyu; Arifin, Nor Anisa; Mardle, Peter; Steinberger-Wilckens, Robert

DOI:
10.1149/2.1011906jes

Document Version
Peer reviewed version

accepted for p[ublication in J of the ECS 2019

Electrochemical Performance and Carbon Resistance Comparison between Tin, Copper and Silver-Doped Nickel/Yttria-Stabilized Zirconia Anodes SOFCs Operated with Biogas

Zeyu Jiang,[z] Nor Anisa Arifin, Peter Mardle, and Robert Steinberger-Wilckens

Centre for Fuel Cell and Hydrogen Research, School of Chemical Engineering, University of Birmingham, Birmingham B15 2TT, United Kingdom

[z]E-mail: aaronjzy35@sina.com

Abstract

Traditional Ni/YSZ anode SOFCs were modified by Sn, Cu and Ag by an infiltration method to obtain Sn-Ni, Cu-Ni and Ag-Ni alloy anode catalysts on the anode. The obtained maximum power density of Ni/YSZ, Sn-doped Ni/YSZ, Cu-doped Ni/YSZ, and Ag-Ni/YSZ cells fuelled by simulated biogas (14 mL min^{-1} CH_4, 7mL min^{-1} CO_2 and 7mL min^{-1} N_2) at 750 ^oC were 0.101, 0.272, 0.085 and 0.102 W cm^{-2} respectively. Stability tests of SOFCs in biogas revealed that the stability of Sn-Ni/YSZ and Ag-Ni/YSZ cells in operation was greatly improved compared to the undoped Ni/YSZ cell. Both Sn-Ni/YSZ and Ag-Ni/YSZ cells stably operated for 48 h, but Ni/YSZ cell ceased operation after 19 h due to carbon deposition. The addition of small amount of Cu did not enhance the anti-coking ability. Other than with the severe carbon deposition on the Ni/YSZ anode surface, no observable fibrous carbon could be identified on the Sn-Ni/YSZ and Ag-Ni/YSZ anode surfaces.

1. Introduction

Solid oxide fuel cells (SOFCs) are classified as high-temperature fuel cells because of their high operating temperature (650-900 ^{o}C). Compare to other fuel cells types, they have several promising advantages: high operating efficiency (55 – 65%), fuel flexibility and high fuel impurity tolerance. The materials used for SOFC manufacturing are normally non-precious metal catalysts and ceramic materials, which greatly reduce the manufacturing cost. Moreover, high-quality waste heat will be generated from the operation of SOFC that can be used for steam generation or as process heat, increasing the fuel cell efficiency to overall 92 to 95%. By using SOFCs to generate electricity, the efficiency of fossil fuel used in the electricity supply system can be significantly increased. Hence, SOFCs have attracted much attention worldwide to reduce the use of fossil fuels [1-4]. Among all hydrocarbon fuels, biogas is a promising candidate, because it is a renewable and environmentally friendly power source that produced from biomass. Biogas mainly consists of CH_4, CO_2, H_2O and trace amount of other contaminants, such as H_2S and NH_3 [5].

Although the nickel cermet anode has excellent catalytic activity to various hydrocarbon fuels, coking and sulphur poisoning are the two most prevalent problems to solve for hydrocarbon fuelled SOFCs. The formation of carbon or NiS compounds can rapidly reduce the cell performance [6, 7]. Nickel can catalyse the methane cracking reaction, Eq. (1), to form hydrogen and solid carbon at the anode of an SOFC. Another carbon forming reaction is the Boudouard Reaction, Eq. (2), which forms carbon below operating temperatures of 600 ^{o}C.

$$CH_4 \rightarrow C + 2H_2 \quad \text{Eq. (1)}$$

$$2CO \rightarrow C + CO_2 \quad \text{Eq. (2)}$$

For the most commonly used Ni/YSZ anode, the deposited carbon is easily dissolved into Ni and then causes volume expansion of the anode material. Because of the good catalytic activity of Ni for carbon formation reactions, the carbon filaments are easily formed on the anode. The accumulation of carbon could lead to serious structural damage of the anode or catalyst deactivation, which drastically reduces the cell performance during operation [3, 8].

In order to enhance the electrochemical performance and carbon resistance of SOFCs operated under hydrocarbon fuels, a lot of studies have been conducted to modify nickel with other materials. Alloying Ni with a small amount of noble metals may enhance the catalytic activity and carbon resistance during the hydrocarbon fuelling. Pt, Pd, Au, Ru, and Ag have been alloyed with Ni by various methods, such as impregnation, in-situ combustion, infiltration, electroless plating, and electrodeposition. Au-Ni anode showed significant enhancement of carbon resistance and operating stability [9, 10]. Pd impregnated Ni/YSZ anodes exhibited lower resistance and suppression of carbon deposition under hydrocarbon fuels [11, 12]. The addition of Ru or Ag to Ni bulk anode also greatly improved the anti-coking ability and operation stability under hydrocarbon fuels[13-16]. Moreover, base metals (Co, Fe, Sn, and Cu) modified Ni anodes have been extensively investigated to reduce the coking problem on the anode. However, the introduction of most base metals to Ni reduced the electrocatalytic activity compared to pure Ni electrocatalyst. A Ni-Co alloy electrocatalyst was found to produce a higher exchange current density in syngas than in pure H_2 with no visible carbon observed on the anode after cell testing [17]. Among those base metals, low concentration Sn-doped Ni anodes showed the most advantageous performance and carbon resistance under hydrocarbon fuels [18-21]. In addition, less carbon was formed on the Cu-Ni anode SOFC than on Ni only anode SOFC when exposed to methane [22-24].

In the work presented here, traditional Ni/YSZ SOFCs were manufactured via aqueous tape casting and then painted with an LSM cathode [25, 26]. After cell manufacturing, these Ni/YSZ anode SOFC cells were modified by Sn, Cu, and Ag particles using an infiltration method. The prepared SOFCs were tested on hydrogen and then simulated biogas at 750 ^{o}C [19]. The electrochemical performance, carbon tolerance, operation stability and resistance were compared between Ni/YSZ cells with different dopant materials.

2. Experimental

2.1. Cell fabrication

Anode-supported button SOFC button cells were used for this study. The anode of the fabricated cell had two layers: the anode substrate (AS) and the anode functional layer (AFL). The anode slurries had a mass ratio of NiO:YSZ 65:35. The solid loading for the anode slurries was 55 wt.%. Because of the difference in function between the two anode layers, two different sizes of NiO powder were used in slurry preparation. For the AS slurry, NiO powder (NiO, Hart Materials) with an average particle diameter of 1-2 µm and pre-calcined (800 ^{o}C in air for 4 h) 8 mol% yttrium stabilized zirconia (TZ-8YS, TOSOH) powder were used. Moreover, 2 wt.% tapioca starch was added into the slurry as the pore former to create a more porous anode surface. For the AFL, finer NiO powder (NiO, PI-KEM) with an average particle diameter of 0.7 µm and the same YSZ powder as in the AS slurry were used. The powder mixtures were ball milled with distilled water and dispersant Dispex® Ultra FA 4404 (BASF) for 24 h. After 24 h of mixing, polyvinyl alcohol solution (PVA 87-90 % hydrolyzed, Sigma-Aldrich) and glycerol (99.5% Glycerol bidistilled, VWR^{TM}) were added into the mixture as binder and moisturizer, respectively. Antifoam 204 (Sigma-Aldrich) was added to reduce the amount of foam. The AS and AFL slurries were filtered after another 12 h mixing of ball milling. The anode slurries were ready to use after 24 h de-airing.

With 50 wt.% the electrolyte slurry solid loading was slightly lower compared to the anode slurries. Water, dispersant (DS001, Polymer Innovations), binder (WB4101, Polymer Innovations), defoamer (DF002, Polymer Innovations), and plasticizer (PL005, Polymer Innovations) were mixed for 24 h. Then, YSZ powder was added into the mixture for another 4 h mixing. As the viscosity of the electrolyte slurry was much lower than that of the anode slurries, the filtered electrolyte slurry was ready for tape casting after 30 min de-airing.

The electrolyte was deposited as the first layer of the multilayer tape by applying it on a PET film (silicone coated) using a long tape casting vacuum coater (MTI Corporation). After

drying at 70 ^{o}C for 15 min, the AFL was applied on the electrolyte layer and then dried at 70 ^{o}C for 15 min. The final layer was the thick anode substrate, which was dried overnight in a vacuum oven at 35 ^{o}C. The dried green tape was cut into pre-sintered half cells with a diameter of 3.5 cm. Then, NiO-YSZ half cells with a diameter of 2.5 cm were obtained after co-sintering in air at 1350 ^{o}C for 4 h.

The cathode pastes for the double-layer cathode were prepared by three-roll milling. The cathode paste for the first layer was LSM ($La_{0.80}Sr_{0.20}$Mn Oxide, Praxair)-YSZ paste with a weight ratio of 50:50. The second layer of the cathode was pure LSM. Both layers were brush-painted onto the electrolyte and then sintered in air at 1100 ^{o}C for 4 h. Figure 1 shows the anode, electrolyte and cathode of the manufactured single cell.

Sn, Cu and Ag were doped on the Ni/YSZ anode by an infiltration method. The target doping metal loadings were 1 wt.% with respect to Ni. $SnCl_2$•$2H_2O$ (Fisher Scientific), $Cu(NO_3)_2$•$3H_2O$ (Acros Organics) and $AgNO_3$ (Acros Organics) were used as the precursor for Sn, Cu and Ag, respectively. In order to infiltrate the dopant into the bulk Ni/YSZ anode, the precursor powder was dissolved in 50% ethanol and 50% water [19]. Then, the required amount of solution was added to the bulk anode's surface with a SciPette pipette (SciQuip). After drying at room temperature, the dried infiltrated cells were calcined in air (the temperature specified in Table 1) for 3 h. The calcined anode surfaces can be shown in Figure 2.

2.2. Cell testing and cell characterization

SOFC with Ni/YSZ anodes were tested at 750 ^{o}C in a horizontal split tube furnace (Vecstar). Hydrogen and simulated biogas were used as the fuel during cell testing. For hydrogen-fuelled cell testing, the flowrates of H_2 and N_2 were 21 mL min^{-1} and 7 mL min^{-1}, respectively. For biogas mode operation, the flowrates of dry CH_4, CO_2 and N_2 were 14 mL min^{-1}, 7 mL min^{-1} and 7 mL min^{-1}, respectively. The current collectors used were silver wires (Scientific Wire Company) that were attached on both anode and cathode by using silver paste (DAD-87, Shanghai Research Institute of Synthetic Resins). The silver paste was also used to seal the cells in alumina testing tubes for further electrochemical testing. The cathode of the button cell was exposed to air in the furnace. The button cells were characterized by OCV, i-V, potentiostatic and EIS characterisations using Solartron 1470E and 1455 FRA analyser (Solartron Analytical). For the AC impedance test, the frequency ranged from 0.1 Hz to 10^6 Hz, with a signal amplitude of 10 mV. The microstructure of the SOFCs was characterized using scanning electron microscopy (SEM) with a Hitachi Tabletop Microscope TM3030 Plus. Element distribution on the anode was analysed by energy-dispersive X-ray spectroscopy (Quantax, Bruker). The dopant element surface concentrations were further analysed by X-ray photoelectron spectroscopy (XPS, HarwellXPS).

3. Results and discussion

3.1. Microstructure of the manufactured cell

Figure 3 shows the SEM images of the fabricated anode-supported SOFC cell anodes, cathodes, and cross sections. Figure 3 (a) and (b) represent the porous Ni/YSZ surface before reduction and after 24 h operation on H_2, respectively. The NiO particles were reduced to Ni particles with the diameter from 0.5 to 1 μm under hydrogen atmosphere. It can be seen from the cross-sectional SEM images of the single cell, Figure 3 (c) and (d), that both electrodes were porous, which allowed fuel and air to permeate. An anode functional layer was added between the bulk Ni/YSZ anode and electrolyte to reduce the

146 interfacial resistance and increase the number of active sites. Moreover, the addition of an
147 AFL improved the cell performance because of the increased number of active sites in the
148 anode [18, 25]. The thickness of the electrolyte, double-layer cathode and anode substrate
149 were about 10, 20 and 700 μm post-sintering, respectively.

150 Figure 4 shows the distribution of Ni, Sn, Cu, and Ag on the anode surfaces of unreduced
151 cells in SEM images and EDX spectra. It can be seen that NiO and YSZ powders were well
152 dispersed during the mixing process. Hence, a uniform distribution of NiO and YSZ was
153 obtained. In addition, for Sn, Cu, and Ag-doped Ni/YSZ anodes, Sn, Cu, and Ag elements on
154 the anode surface were SnO_2, CuO, and Ag particles after the thermal decomposition of
155 dopant precursors, respectively [13, 27, 28]. The mass ratio of Sn, Cu, and Ag to Ni on the
156 anode surfaces measured by EDX were 3.90, 3.27 and 43.38 wt.%, respectively. The
157 dopants preferentially remained on the surface of the Ni/YSZ anode, especially in the case
158 of Ag particles. The $AgNO_3$ was decomposed to Ag directly, but other dopants were
159 decomposed to oxides. Therefore, Ag had the highest concentration on the Ni/YSZ anode
160 surface.

161 Figure 5 (a), (b), and (c) show the microstructure of the H_2 reduced Sn, Cu, and Ag-doped
162 anodes, respectively. Compared with the unreduced anodes in Figure 4, it can be seen that
163 the H_2 reduced anodes possessed higher porosity. More importantly, the metal catalyst
164 particles can be observed from the porous anodes surface, especially the large Ag particles.
165 XPS analysis was also performed to the H_2 reduced Ni/YSZ, Sn-Ni/YSZ, Cu-Ni/YSZ, and
166 Ag-Ni/YSZ anodes surface. The XPS survey spectrums of the H_2 reduced anodes are shown
167 in Figure 6. The metallic elements on the anode surface were well identified by XPS. Table 2
168 shows the surface concentrations of the dopant elements on the anode surface. Compared
169 to the surface concentration of the dopant elements measured by EDX, the mass ratio of Sn,
170 Cu, and Ag to Ni on the anode surfaces measured by XPS were much higher, 193.65, 11.70,
171 and 2879.63 wt.%, respectively. The significantly increased dopant concentration on the
172 anode surface could be explained by the ultra-thin analysis depth of XPS. The results

obtained from XPS further proved that the dopant preferentially remained on the surface of anode.

3.2. Electrochemical performance

Figure 7 shows the i-V characterization of the tested cell on H_2 and biogas. According to the obtained i-V curves, the maximum power density of undoped Ni/YSZ single cell on H_2 and biogas was 0.263 W cm^{-2} and 0.101 W cm^{-2}, respectively. The OCV produced from H_2 fuelled single cells was 1.08 V, which is close to the theoretical value at this temperature (1.12 V). The reason why experimental OCV values were slightly lower than the theoretical value might be attributed to the crossover of gases or incomplete sealing between the cell and cell holder. However, the OCV produced from the biogas fuelled single cell slightly decreased to 1.02 V due to the different fuel composition with an inert CO_2 component. During methane dry reforming, the amount of hydrogen produced from the reforming reactions will be less than that in a pure hydrogen fuel. Consequently, the electrochemical performance of the single cell was much lower on biogas than on pure hydrogen.

For 1 wt.% Sn-doped Ni/YSZ anode SOFC, the profiles of current density on both fuels are similar, with the maximum power density of 0.280 and 0.272 W cm^{-2} on H_2 and biogas respectively. The OCV produced from the biogas fuelled single cell (1.07 V) was slightly higher than that of the H_2 fuelled cell (1.05 V) and the performances were very similar. This improved cell performance on biogas has also been observed in previous studies [18, 19, 21]. Although the performance of the cell on hydrogen was slightly better than that of on biogas, the addition of 1 wt.% Sn on the anode greatly enhanced the cell performance on biogas. In contrast, as shown in the graphs, the maximum power densities of the 1 wt.% Cu-doped Ni/YSZ anode SOFC on H_2 and biogas were 0.286 and 0.085 W cm^{-2}, respectively. The addition of Cu to the Ni/YSZ anode reduced the cell performance on biogas fuel. However, the cell performance on H_2 had a small increment. The obtained results were similar to the work done by Rismanchian et al. [22]. In their experiment, electroless plated Cu-Ni/YSZ anodes were tested on dry methane and showed lower performance than that of

200 traditional Ni/YSZ anodes at the same temperature. The reduced performance can be
201 explained by the formation of a Cu-Ni alloy on the anode surface that blocks Ni active sites
202 [22]. Compared with undoped Ni/YSZ cells, Ag-Ni/YSZ cells on biogas showed very similar
203 performance to Ni/YSZ cells. Nevertheless, the cells had very competitive performances with
204 maximum power density of 0.313 W cm^{-2} when H_2 was used as the fuel. The maximum
205 power density of the single cell on biogas was 0.102 W cm^{-2}, which was slightly higher than
206 that of undoped and Cu-doped cells. In contrast to the Ag-impregnated Ni/YSZ anode from
207 the work of Wu et al. [14], the addition of Ag particles via the infiltration method did not
208 enhance or reduce the cell performance on biogas. This might be attributed to the lower
209 amount of Ag particles on the anode surface or the poor formation of Ag-Ni alloy in the bulk
210 anode [14].
211
212 The electrochemical impedance spectra of the single cells fuelled by H_2 and biogas obtained
213 at 0.7 V from 10^6 Hz to 0.1 Hz can be seen in Figure 8. For H_2 fuelled single cells, the ohmic
214 resistance of SOFC with Ni/YSZ, Sn-doped Ni/YSZ, Cu-doped Ni/YSZ and Ag-doped Ni/YSZ
215 cells was 0.11, 0.08, 0.08, and 0.08 Ω cm^2, respectively. Apparently, the undoped Ni/YSZ
216 cell has the highest ohmic resistance compare to the other cells. The declined ohmic
217 resistance of the modified anodes could be explained by the addition of Sn, Cu, and Ag on
218 the anodes improved the electronic conductivity of the electrode. The overall electrode
219 polarisation resistance was 0.50, 0.37, 0.38, and 0.43 Ω cm^2. It can be seen from Figure 6 (a)
220 that the Ag-decorated cell had higher polarization resistance than Sn-Ni and Cu-Ni cells.
221 Large Ag particles on the anode are likely to block the fuel transportation channel on the
222 porous anode, which lead to the increased total resistance. When H_2 was used as the fuel,
223 both ohmic and electrode resistances for the doped cells were lower than those of undoped
224 Ni/YSZ cells. The decreased ohmic resistance and electrode polarization resistance of the
225 doped cells could be attributed to the increase in electronic conductivity and catalytic activity
226 of the bulk anode from the addition of Sn, Cu, or Ag particles. As shown in the graph, the
227 overall cell resistance increased remarkably when biogas was used as fuel. Due to the

change of fuel type at the anode, the anode polarization results in the shift of impedance arcs [29]. The biogas fuelled cells showed the same ohmic resistance values as H_2-fuelled cells, but the electrode polarization resistances were higher than for H_2 fuel. It can be seen that the total polarization resistance of the Sn-Ni cell increased from 0.37 Ω cm^2 in H_2 to 0.45 Ω cm^2 in biogas, which was the lowest among all measured cells. A possible reason could be the enhanced catalytic activity of Sn-Ni on methane reforming reactions. Among these single cells, the 1 wt.% Sn-doped Ni/YSZ anode SOFC showed the minimum total resistance on both H_2 and biogas. The difference of the impedance results between Sn-Ni anode and the other anodes can be explained by the high catalytic activity of Sn as electrochemical catalyst at the anode during biogas operation.

3.3. Long-term stability of the single cells fuelled by biogas

The effect of the dopants on the Ni/YSZ anode might change over the operating time of the SOFC. Hence, galvanostatic experiments were conducted to investigate the cell stability under biogas fuel. A constant current density of 0.2 A cm^{-2} was applied to each single cell for 48 hours. The 48-hour cell stability test on biogas and AC impedance results can be seen in Figure 9. Clearly, the Sn-doped SOFC exhibited extraordinary performance with a low degradation rate of 2.98×10^{-4} V h^{-1} compare to the other single cells. The Ag-doped cell showed voltage fluctuations during operation with a slightly higher degradation rate of 7.93×10^{-4} V h^{-1}. Nevertheless, the cell performance of the pure Ni/YSZ anode cell degraded rapidly and then ceased operation after 19h.The voltage of the Cu-doped cell dropped to 0.2 V at the beginning and then increased to 0.34 V after 5 h exposure to biogas. However, the measured voltage of the Cu-doped cell dropped to 0.025 V at the end of the galvanostatic test. Compared to the other doped cells, the Cu-doped cell had the most unstable performance and the highest degradation rate of 6.2×10-3 V h^{-1}. According to the obtained results, the long-term stability of the cell under biogas could be significantly improved by the addition of 1 wt.% Sn or Ag to the Ni/YSZ bulk anode. Impedance analysis for each single cell was performed after 2 h and 50 h galvanostatic operation under biogas with current

density of 0.2 A cm^{-2}. The ohmic resistance of the cells were the same at 2 h and 50 h biogas operation, but the total polarization resistances all showed a rising trend. The Ni/YSZ cell showed the highest total resistance among all tested cells during biogas operation. The electrode resistance of Sn-Ni/YSZ cells had a small increase from 0.44 to 0.50 Ω cm^2. For Cu-Ni/YSZ and Ag-Ni/YSZ cells, the obtained impedance results were very similar after both 2 h and 50 h operation under biogas. The increase in polarization resistance could be explained by the accumulation of carbon on the anode resulted in anode catalyst degradation.

3.4. Carbon deposition on the anode surface

The elements on the anode surface were quantified by the EDX using weight percent after measuring the morphology of the anode surface, which could be shown as Table 3. It can be seen that the pure Ni/YSZ SOFC had the highest level of carbon on the anode surface. The anodes treated with Sn, Cu, and Ag all exhibited less carbon on the anode surface than that of the traditional Ni/YSZ anode. The measured area of the Ag-Ni anode surface showed only 0.34 wt.% Ag:Ni mass ratio. This can be explained by the uneven distribution of dopant on the surface during the infiltration process and a subsequently inhomogeneous distribution of Ag particles infiltrated into the anode matrix, or by volatilisation of Ag during high temperature operation.

Figure 10 shows SEM images of the anodes after cell test at 750 ^oC. Many amorphous and fibrous carbons deposits are seen on the Ni/YSZ and Cu-Ni/YSZ anodes after 24 h exposure to biogas but no carbon wires were observed. The accumulation of carbon destroyed the structure of the Ni catalyst and resulted in significantly reduced cell performance. Furthermore, severe coking problem can result in the anode expansion, leading to cell cracking [30]. In contrast, there were no observable carbon fibres on Sn-Ni/YSZ and Ag-Ni/YSZ anodes. Therefore, alloying Sn or Ag with Ni electrochemical catalysts successfully suppressed the accumulation of carbon on the anode surface of biogas fuelled SOFCs.

4. Conclusion

1 wt.% Sn, Cu and Ag-doped Ni/YSZ anodes were fabricated via an infiltration method and their electrochemical performance, operation stability and carbon resistance were compared to Ni/YSZ anodes. The infiltrated Sn, Cu and Ag particles preferentially remained on the Ni/YSZ anode surfaces. Compared to the traditional Ni/YSZ anode SOFC, both 1 wt% Sn-doped and 1 wt.% Ag-doped Ni/YSZ anode SOFCs showed enhanced operational stability and resistance to coking under simulated biogas fuel at 750 ^{o}C operating temperature. Moreover, no fibrous carbon could be observed on the anode surfaces of Sn-Ni/YSZ and Ag-Ni/YSZ cells. It is also worth mentioning that the addition of a small quantity of Ag particles to Ni/YSZ greatly increased the cell performance under H_2 fuel. However, the presence of 1 wt.% Cu did not lead to a significant suppression of carbon formation on Ni/YSZ anodes and any improvement of operational stability. The cell performance of Cu-Ni/YSZ anodes was even lower than that of Ni/YSZ anode on biogas fuel. Considering the issues of evaporation with Cu and Ag, Cu-Ni/YSZ and Ag-Ni/YSZ anode cells might have better electrochemical performance at intermediate operating temperature.

Acknowledgements

This work was supported by Centre for Fuel Cell and Hydrogen Research, Birmingham, United Kingdom. The authors thanks Dr. Artur Majewski and Dr. Lina Troskialina for helpful discussions.

References

[1] X.-M. Ge, S.-H. Chan, Q.-L. Liu, and Q. Sun, "Solid Oxide Fuel Cell Anode Materials for Direct Hydrocarbon Utilization," *Advanced Energy Materials,* vol. 2, no. 10, pp. 1156-1181, 2012.

[2] W. Wang, C. Su, Y. Wu, R. Ran, and Z. Shao, "Progress in Solid Oxide Fuel Cells with Nickel-Based Anodes Operating on Methane and Related Fuels," *Chemical Reviews,* vol. 113, no. 10, pp. 8104-8151, 2013/10/09, 2013.

[3] P. Boldrin, E. Ruiz-Trejo, J. Mermelstein, J. M. Bermúdez Menéndez, T. Ramírez Reina, and N. P. Brandon, "Strategies for Carbon and Sulfur Tolerant Solid Oxide Fuel Cell Materials, Incorporating Lessons from Heterogeneous Catalysis," *Chemical Reviews,* vol. 116, no. 22, pp. 13633-13684, 2016/11/23, 2016.

[4] K. Kendall, and M. Kendall, *High-Temperature Solid Oxide Fuel Cells for the 21st Century: Fundamentals, Design and Applications: Second Edition*, London: Elsevier, 2015.
[5] B. Hua, M. Li, Y.-F. Sun, Y.-Q. Zhang, N. Yan, J. Chen, J. Li, T. Etsell, P. Sarkar, and J.-L. Luo, "Biogas to syngas: flexible on-cell micro-reformer and NiSn bimetallic nanoparticle implanted solid oxide fuel cells for efficient energy conversion," *Journal of Materials Chemistry A,* vol. 4, no. 12, pp. 4603-4609, 2016.
[6] Z. Tao, G. Hou, N. Xu, and Q. Zhang, "A highly coking-resistant solid oxide fuel cell with a nickel doped ceria: Ce1−xNixO2−y reformation layer," *International Journal of Hydrogen Energy,* vol. 39, no. 10, pp. 5113-5120, 2014/03/26/, 2014.
[7] Y. Jiao, L. Zhang, W. An, W. Zhou, Y. Sha, Z. Shao, J. Bai, and S.-D. Li, "Controlled deposition and utilization of carbon on Ni-YSZ anodes of SOFCs operating on dry methane," *Energy,* vol. 113, pp. 432-443, 2016/10/15/, 2016.
[8] H. Kan, S. H. Hyun, Y.-G. Shul, and H. Lee, "Improved solid oxide fuel cell anodes for the direct utilization of methane using Sn-doped Ni/YSZ catalysts," *Catalysis Communications,* vol. 11, no. 3, pp. 180-183, 2009/11/25/, 2009.
[9] I. A. Proctor, A. L. Hopkin, and R. M. Ormerod, "Development of anodes for direct electrocatalytic oxidation of methane in solid oxide fuel cells," *Ionics,* vol. 9, no. 3, pp. 242-247, 2003/05/01, 2003.
[10] D. K. Niakolas, J. P. Ouweltjes, G. Rietveld, V. Dracopoulos, and S. G. Neophytides, "Au-doped Ni/GDC as a new anode for SOFCs operating under rich CH4 internal steam reforming," *International Journal of Hydrogen Energy,* vol. 35, no. 15, pp. 7898-7904, 2010/08/01/, 2010.
[11] A. Babaei, S. P. Jiang, and J. Li, "Electrocatalytic Promotion of Palladium Nanoparticles on Hydrogen Oxidation on Ni/GDC Anodes of SOFCs via Spillover," *Journal of the Electrochemical Society* vol. 156, pp. B1022-B1029, 2009.
[12] A. Babaei, and S. P. jiang, "Analysis of Fuel Oxidation Reaction Steps in Ni/GDC Anode Electrode of Solid Oxide Fuel Cells by Using Palladium Nanoparticles," *Proc. SPIE* vol. 7743, 2010.
[13] X. Wu, X. Zhou, Y. Tian, X. Kong, J. Zhang, W. Zuo, X. Ye, and K. Sun, "Preparation and electrochemical performance of silver impregnated Ni-YSZ anode for solid oxide fuel cell in dry methane," *International Journal of Hydrogen Energy,* vol. 40, no. 46, pp. 16484-16493, 2015/12/14/, 2015.
[14] X. Wu, Y. Tian, J. Zhang, W. Zuo, X. Kong, J. Wang, K. Sun, and X. Zhou, "Enhanced electrochemical performance and carbon anti-coking ability of solid oxide fuel cells with silver modified nickel-yttrium stabilized zirconia anode by electroless plating," *Journal of Power Sources,* vol. 301, pp. 143-150, 2016/01/01/, 2016.
[15] I. Gavrielatos, D. Montinaro, A. Orfanidi, and S. Neophytides, "Thermogravimetric and Electrocatalytic Study of Carbon Deposition of Ag‐doped Ni/YSZ Electrodes under Internal CH4 Steam Reforming Conditions," *Fuel Cells,* vol. 9, no. 6, pp. 883-890, 2010.
[16] T. Hibino, A. Hashimoto, M. Yano, M. Suzuki, and M. Sano, "Ru-catalyzed anode materials for direct hydrocarbon SOFCs," *Electrochimica Acta,* vol. 48, no. 17, pp. 2531-2537, 2003/07/15/, 2003.
[17] J. S. O'Brien, and J. B. Giorgi, "Solid oxide fuel cell with NiCo–YSZ cermet anode for oxidation of CO/H2 fuel mixtures," *Journal of Power Sources,* vol. 200, pp. 14-20, 2012/02/15/, 2012.
[18] H. Kan, and H. Lee, "Sn-doped Ni/YSZ anode catalysts with enhanced carbon deposition resistance for an intermediate temperature SOFC," *Applied Catalysis B: Environmental,* vol. 97, no. 1, pp. 108-114, 2010/06/09/, 2010.
[19] L. Troskialina, A. Dhir, and R. Steinberger-Wilckens, "Improved Performance and Durability of Anode Supported SOFC Operating on Biogas," *ECS Transactions,* vol. 68, no. 1, pp. 2503-2513, 2015.

[20] E. Nikolla, J. Schwank, and S. Linic, “Direct Electrochemical Oxidation of Hydrocarbon Fuels on SOFCs: Improved Carbon Tolerance of Ni Alloy Anodes,” *Journal of The Electrochemical Society,* vol. 156, pp. B1312-B1316, 2009.
[21] A. Singh, and J. M. Hill, “Carbon tolerance, electrochemical performance and stability of solid oxide fuel cells with Ni/yttria stabilized zirconia anodes impregnated with Sn and operated with methane,” *Journal of Power Sources,* vol. 214, pp. 185-194, 2012/09/15/, 2012.
[22] A. Rismanchian, J. Mirzababaei, and S. S. C. Chuang, “Electroless plated Cu–Ni anode catalyst for natural gas solid oxide fuel cells,” *Catalysis Today,* vol. 245, pp. 79-85, 2015/05/01/, 2015.
[23] M. Liu, S. Wang, T. Chen, C. Yuan, Y. Zhou, S. Wang, and J. Huang, “Performance of the nano-structured Cu–Ni (alloy) -CeO2 anode for solid oxide fuel cells,” *Journal of Power Sources,* vol. 274, pp. 730-735, 2015/01/15/, 2015.
[24] S. Islam, and J. M. Hill, “Preparation of Cu–Ni/YSZ solid oxide fuel cell anodes using microwave irradiation,” *Journal of Power Sources,* vol. 196, no. 11, pp. 5091-5094, 2011/06/01/, 2011.
[25] H. Moon, S. D. Kim, E. W. Park, S. H. Hyun, and H. S. Kim, “Characteristics of SOFC single cells with anode active layer via tape casting and co-firing,” *International Journal of Hydrogen Energy,* vol. 33, no. 11, pp. 2826-2833, 2008/06/01/, 2008.
[26] P. Gannon, S. Sofie, M. Deibert, R. Smith, and V. Gorokhovsky, “Thin film YSZ coatings on functionally graded freeze cast NiO/YSZ SOFC anode supports,” *Journal of Applied Electrochemistry,* vol. 39, no. 4, pp. 497-502, 2009/04/01, 2009.
[27] R. Al-Gaashani, S. Radiman, N. Tabet, and A. R. Daud, “Optical properties of SnO2 nanostructures prepared via one-step thermal decomposition of tin (II) chloride dihydrate,” *Materials Science and Engineering: B,* vol. 177, no. 6, pp. 462-470, 2012/04/15/, 2012.
[28] B. V. L'Vov, and A. V. Novichikhin, “Mechanism of thermal decomposition of hydrated copper nitrate in vacuo,” *Spectrochimica Acta Part B: Atomic Spectroscopy,* vol. 50, no. 12, pp. 1459-1468, 1995/10/01/, 1995.
[29] E. W. Park, H. Moon, M.-s. Park, and S. H. Hyun, “Fabrication and characterization of Cu–Ni–YSZ SOFC anodes for direct use of methane via Cu-electroplating,” *International Journal of Hydrogen Energy,* vol. 34, no. 13, pp. 5537-5545, 2009/07/01/, 2009.
[30] H. He, and J. M. Hill, “Carbon deposition on Ni/YSZ composites exposed to humidified methane,” *Applied Catalysis A: General,* vol. 317, no. 2, pp. 284-292, 2007/02/07/, 2007.

Figure Captions

Figure 1: (a) anode, (b) electrolyte and (c) cathode of the manufactured SOFC

Figure 2: (a) Sn-doped, (b) Cu-doped and (c) Ag-doped Ni/YSZ anode single cell

Figure 3: SEM images of the manufactured anode-supported SOFC: (a) pre-test bulk anode, (b) H_2 reduced bulk anode, (c) pre-test bulk anode, (d) cross section of the SOFC

Figure 4: (b) EDX spectrum for Ni/YSZ, (d) Sn-Ni/YSZ, (f) Cu-Ni/YSZ and (h) Ag-Ni/YSZ anode cells before the test

Figure 5: SEM images of the H_2 reduced (a) Sn-Ni/YSZ, (b) Cu-Ni/YSZ, (c) Ag-Ni/YSZ anodes

Figure 6: XPS elemental analysis results on the biogas tested anodes

Figure 7: I-V characterization measured at 750 ^{o}C for undoped Ni/YSZ, 1 wt.% Sn-doped Ni/YSZ, 1 wt.% Cu-doped Ni/YSZ, 1 wt.% Ag-doped Ni/YSZ anode single cells fuelled by (a) H_2 and (b) dry biogas

Figure 8: Electrochemical impedance spectrum of undoped Ni/YSZ, Sn, Cu and Ag-doped Ni/YSZ anode single cells fuelled by (a) H_2 and (b) biogas

Figure 9: Galvanostatic cell stability test on biogas at 0.2 A cm^{-2} current density and impedance spectrum after 1 h and 50 h exposure to biogas at 750 ^{o}C

Figure 10: SEM pictures of (a) Ni/YSZ, (b) Sn-Ni/YSZ, (c) Cu-Ni/YSZ, (d) Ag-Ni/YSZ anode surfaces after 24 hours biogas exposure at 750 ^{o}C

Table Captions

Table 1: Calcination temperature for the modified doped Ni/YSZ SOFC anodes

423 Table 2 – Surface element concentration on the hydrogen-reduced Sn-Ni, Cu-Ni, and Ag-Ni
424 anodes from XPS

425 Table 3: EDX quantify results for the anode surface of tested Ni/YSZ, Sn, Cu, Ag-doped
426 Ni/YSZ SOFCs after 24 hours biogas operation

427

428 **Tables**

429 *Table 1: Calcination temperature for the modified doped Ni/YSZ SOFC anodes*

Anode material	**Sn-doped Ni/YSZ**	**Cu-doped Ni/YSZ**	**Ag-doped Ni/YSZ**
Precursor material	$SnCl_2 \cdot 2H_2O$	$Cu(NO_3)_2 \cdot 3H_2O$	$AgNO_3$
Calcination temperature / °C	600	400	500

430

431 *Table 2 – Surface element concentration on the hydrogen-reduced Sn-Ni, Cu-Ni, and Ag-Ni anodes from XPS*

Anode type / Element / wt.%	**Sn-Ni/YSZ**	**Cu-Ni/YSZ**	**Ag-Ni/YSZ**
Ni	1.89	14.45	1.62
Sn	3.66	0	0
Cu	0	1.69	0
Ag	0	0	46.65

432

433 *Table 3: EDX quantify results for the anode surface of tested Ni/YSZ, Sn, Cu, Ag-doped Ni/YSZ SOFCs after 24*
434 *hours biogas operation*

Anode type / Element / wt.%	**Ni/YSZ**	**Sn-Ni/YSZ**	**Cu-Ni/YSZ**	**Ag-Ni/YSZ**
O	24.95	17.32	20.42	22.93
Zr	33.96	34.67	37.13	35.71
Y	5.60	5.74	6.29	5.83
C	5.32	4.50	3.61	3.25
Ni	30.16	37.21	31.91	32.17
Sn	0	0.56	0	0
Cu	0	0	0.65	0
Ag	0	0	0	0.11

435

436

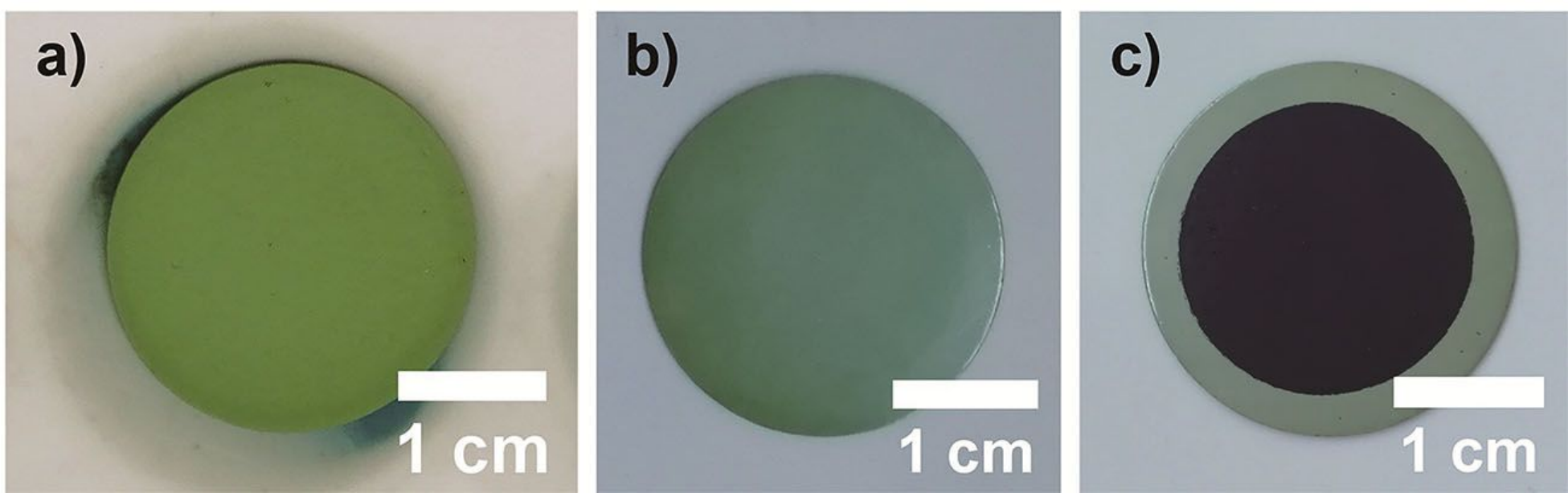
a)
1 cm
b)
1 cm
c)
1 cm

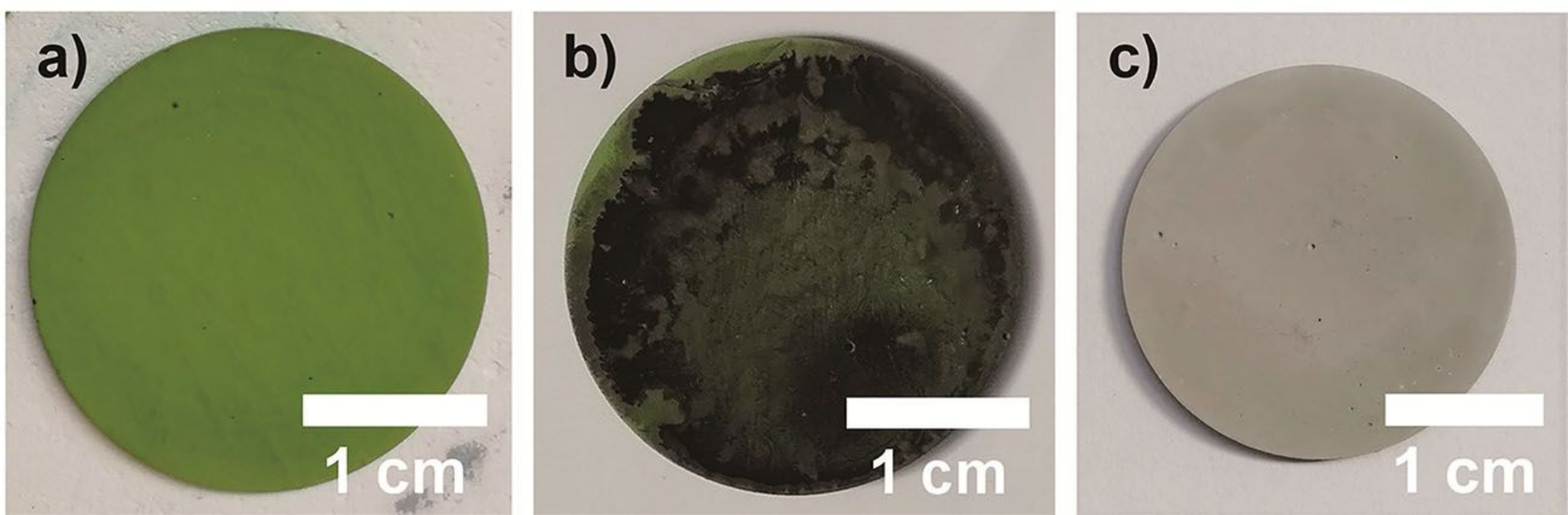
a)
1 cm
b)
1 cm
c)
1 cm

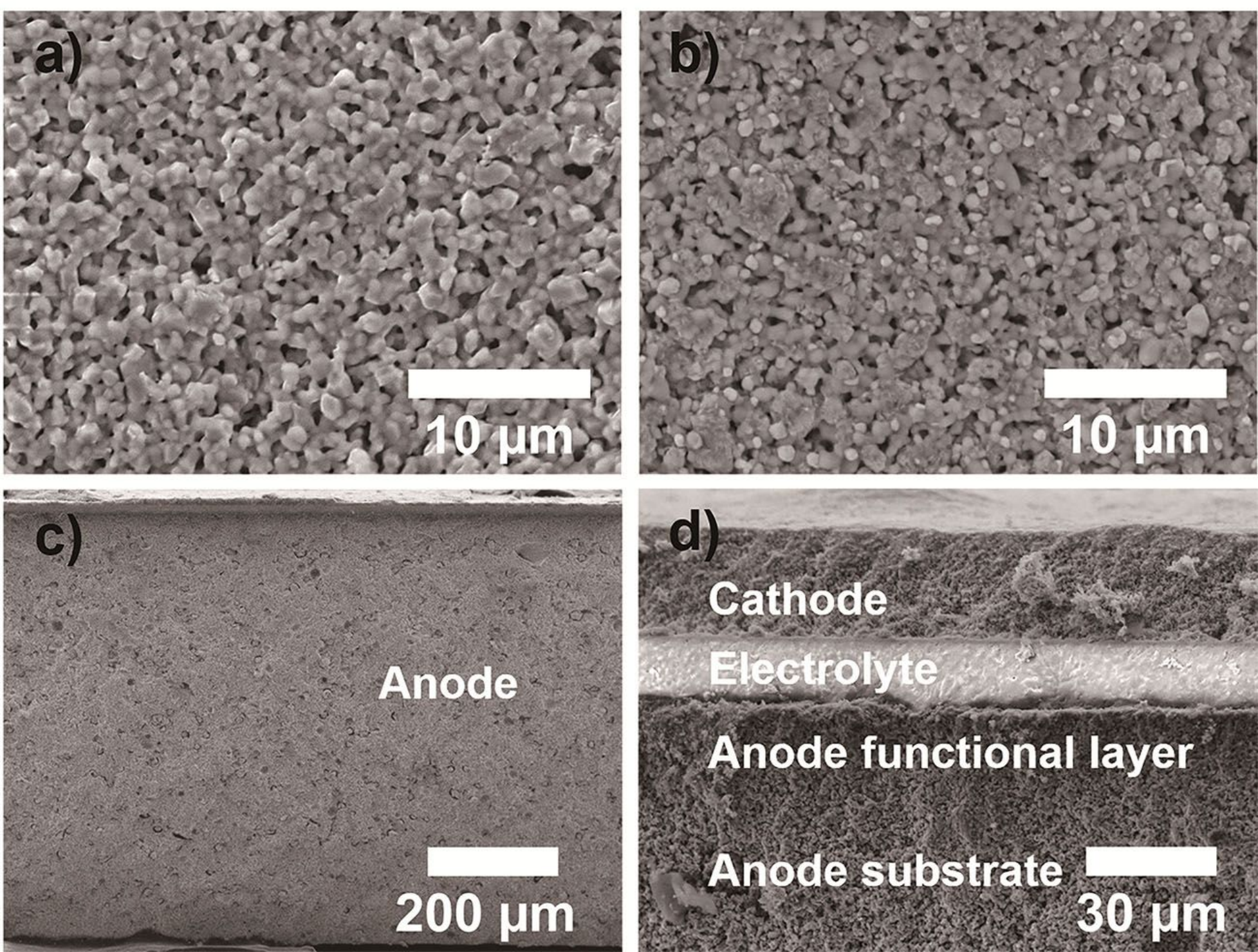
a)
10 µm
b)
10 µm
c)
Anode
200 µm
d)
Cathode
Electrolyte
Anode functional layer
Anode substrate
30 µm

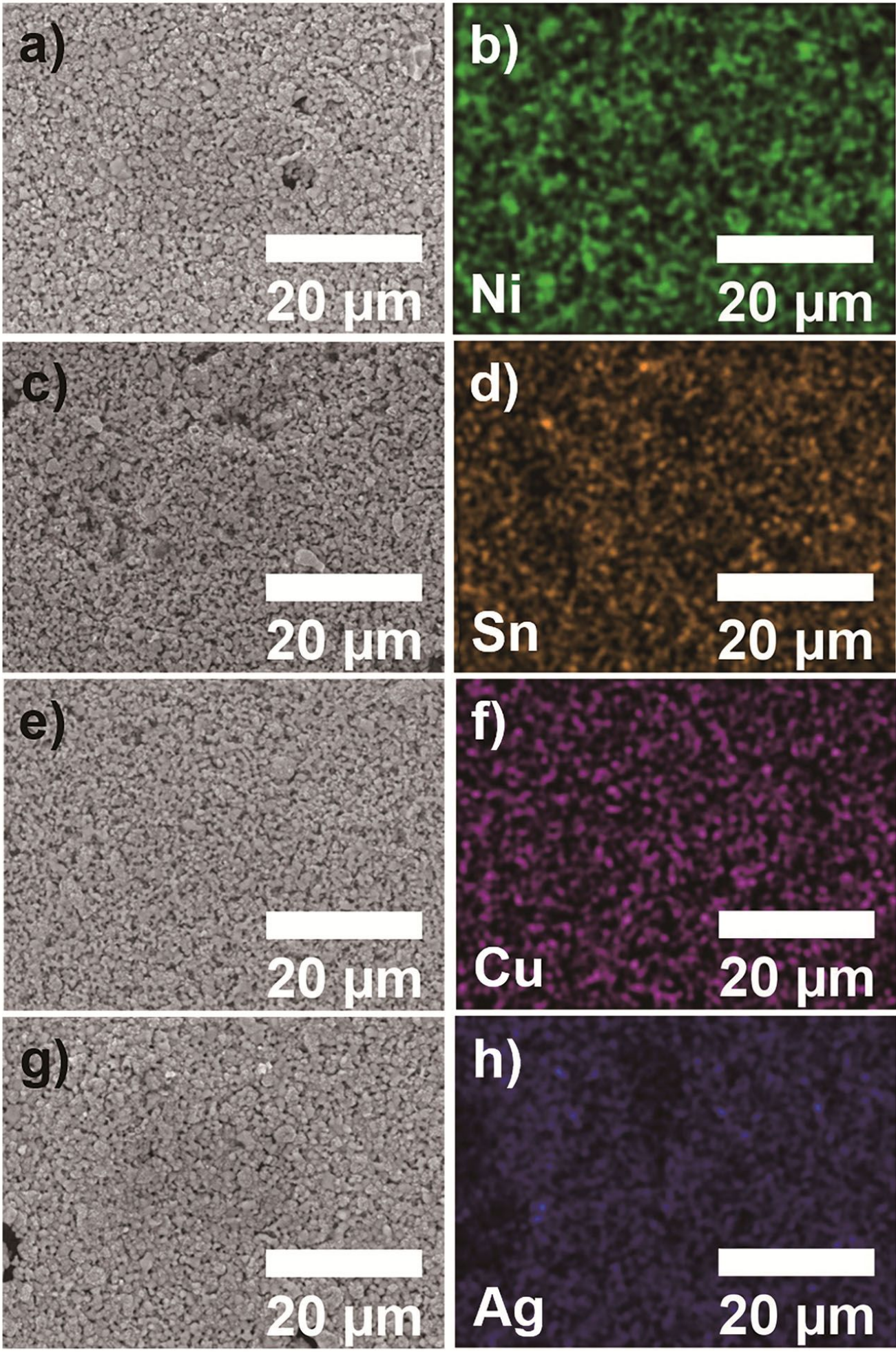
a)
20 µm
b)
Ni
20 µm
c)
20 µm
d)
Sn
20 µm
e)
20 µm
f)
Cu
20 µm
g)
20 µm
h)
Ag
20 µm

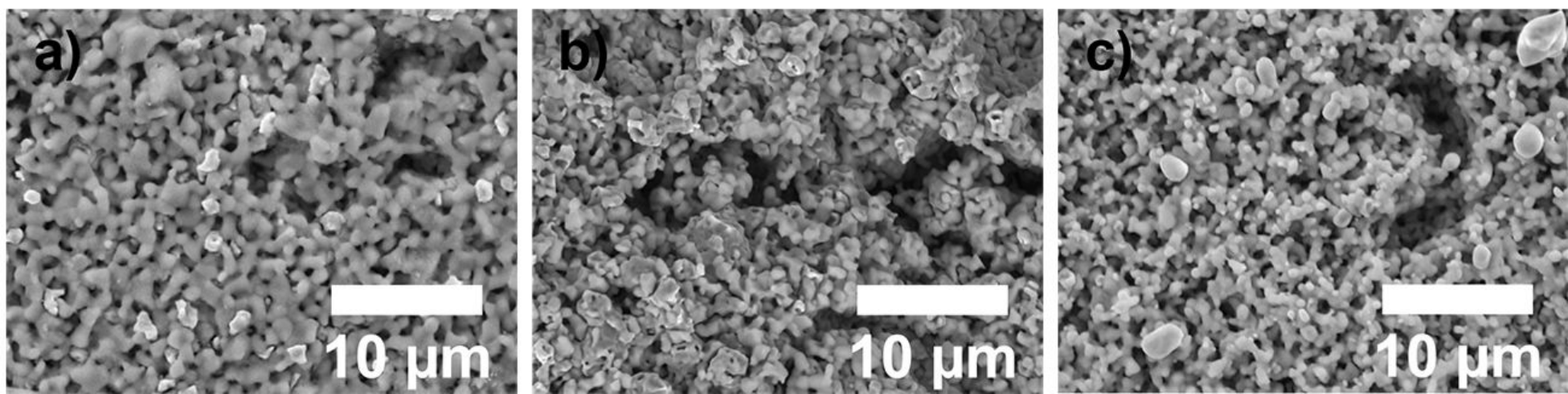
a)
10 µm
b)
10 µm
c)
10 µm

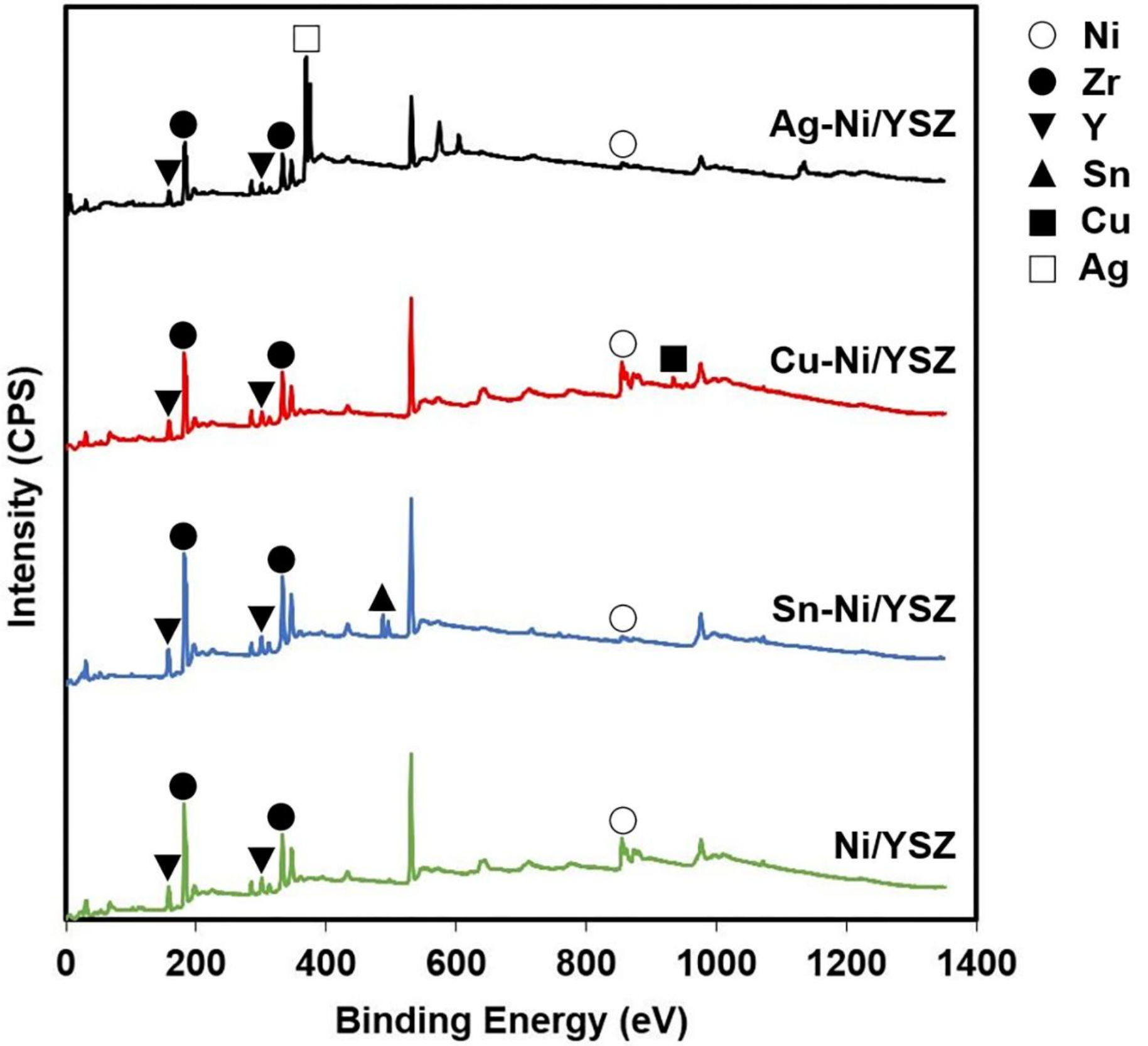
Ni
Zr
Y
Sn
Cu
Ag
Ag-Ni/YSZ
Cu-Ni/YSZ
Sn-Ni/YSZ
Ni/YSZ
Intensity (CPS)
0
200
400
600
800
1000
1200
1400
Binding Energy (eV)

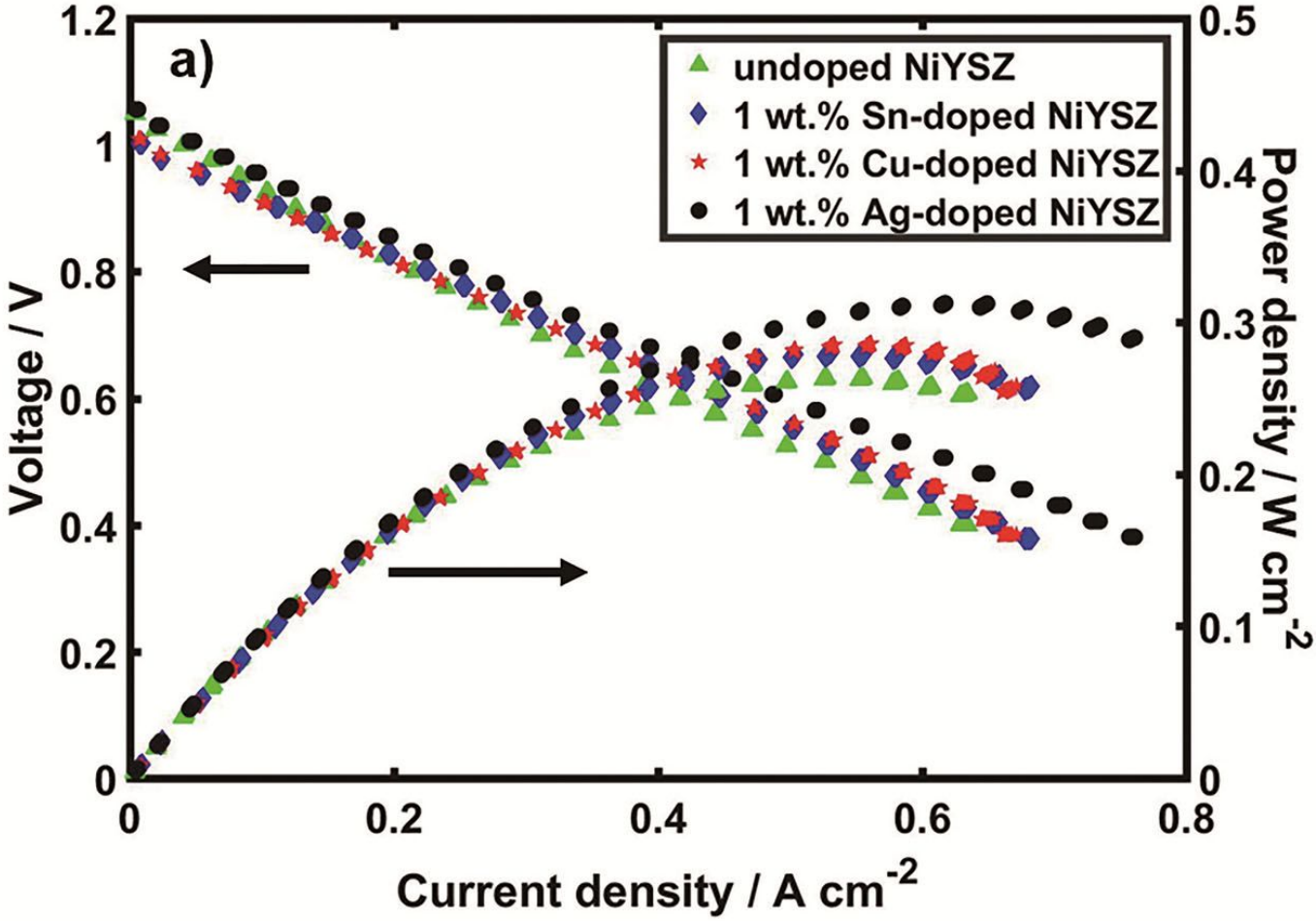
a)
undoped NiYSZ
1 wt.% Sn-doped NiYSZ
1 wt.% Cu-doped NiYSZ
1 wt.% Ag-doped NiYSZ
Voltage / V
Power density / W cm-2
Current density / A cm-2
0
0.2
0.4
0.6
0.8
1
1.2
0.1
0.3
0.5

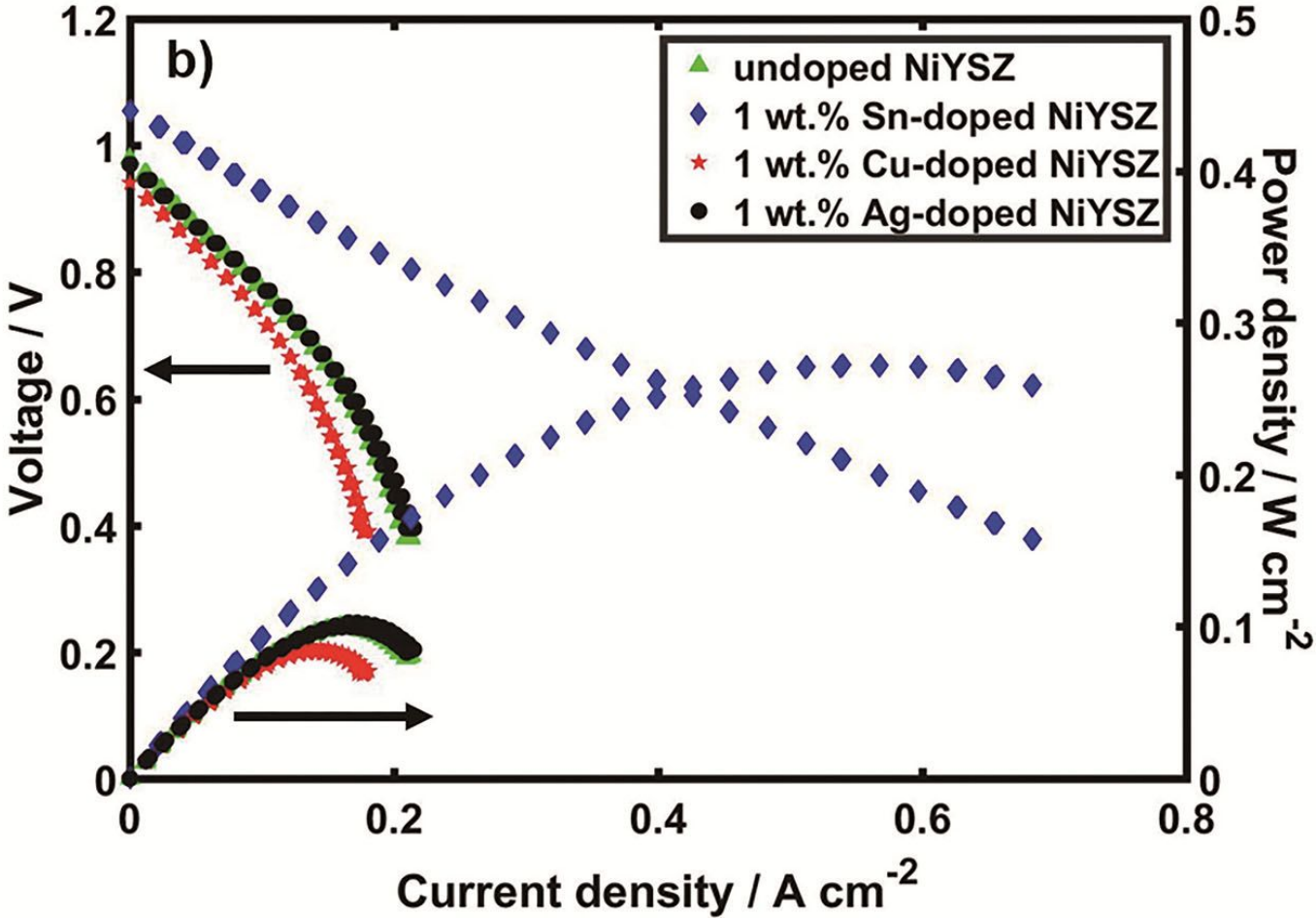
b)
undoped NiYSZ
1 wt.% Sn-doped NiYSZ
1 wt.% Cu-doped NiYSZ
1 wt.% Ag-doped NiYSZ
Voltage / V
Power density / W cm-2
Current density / A cm-2
0
0.2
0.4
0.6
0.8
1
1.2
0.1
0.3
0.5

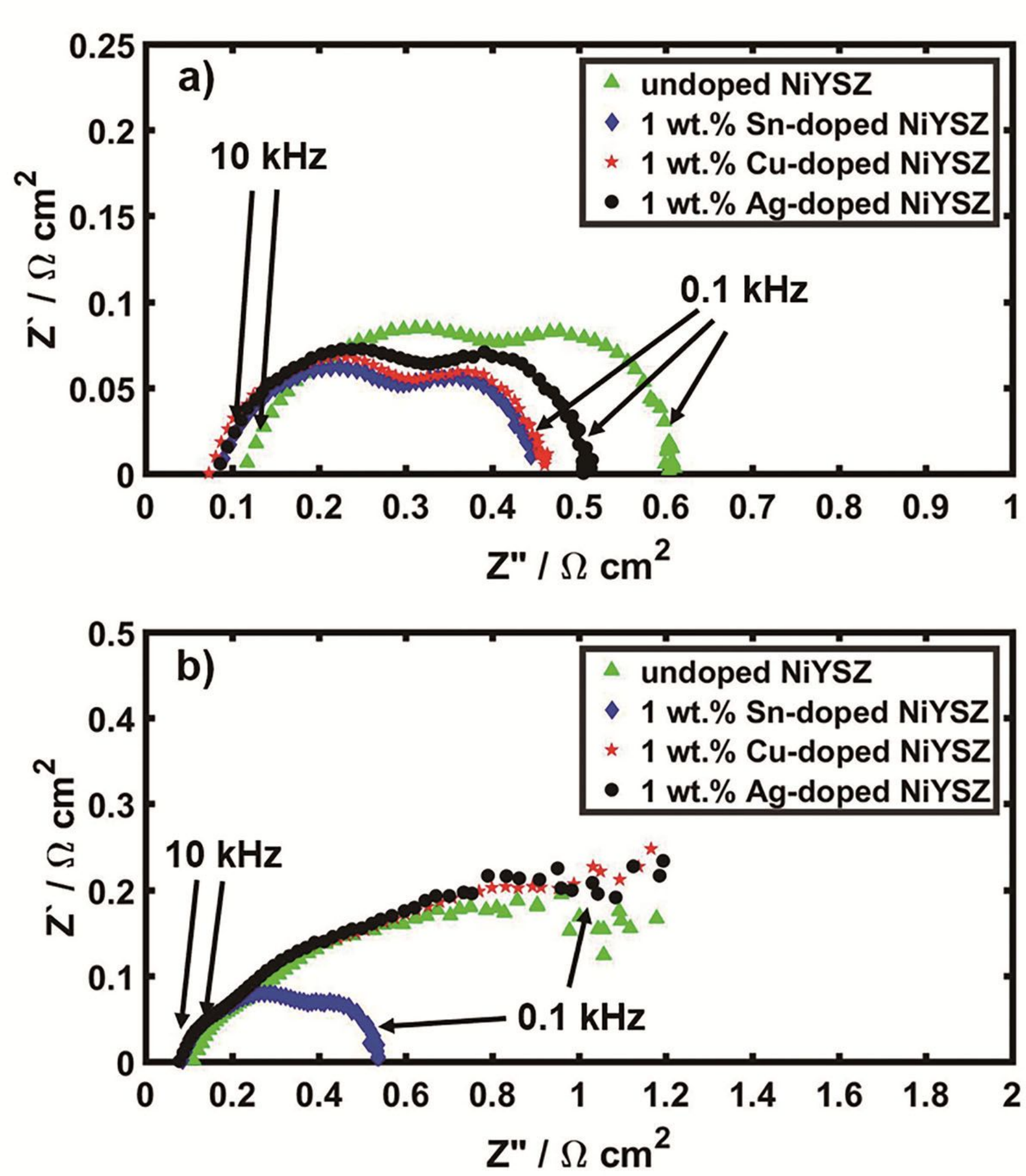
a)
undoped NiYSZ
1 wt.% Sn-doped NiYSZ
1 wt.% Cu-doped NiYSZ
1 wt.% Ag-doped NiYSZ
10 kHz
0.1 kHz
Z` / Ω cm2
Z" / Ω cm2
0
0.05
0.1
0.15
0.2
0.25
0.1
0.2
0.3
0.4
0.5
0.6
0.7
0.8
0.9
1
b)
undoped NiYSZ
1 wt.% Sn-doped NiYSZ
1 wt.% Cu-doped NiYSZ
1 wt.% Ag-doped NiYSZ
10 kHz
0.1 kHz
Z` / Ω cm2
Z" / Ω cm2
0
0.1
0.2
0.3
0.4
0.5
0.2
0.4
0.6
0.8
1
1.2
1.4
1.6
1.8
2

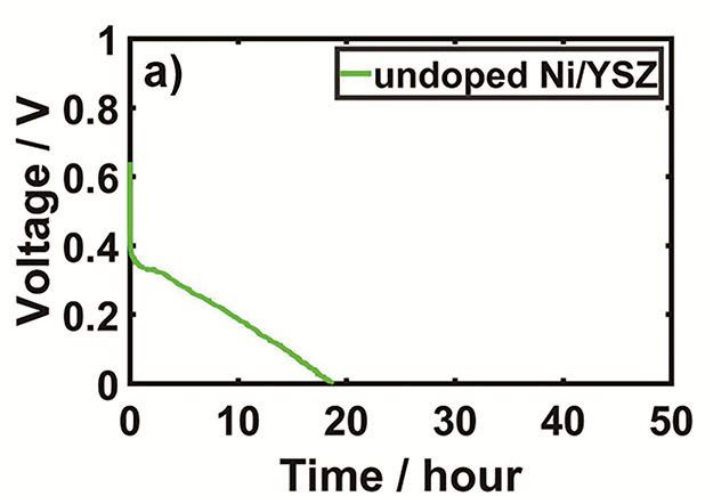
a)
undoped Ni/YSZ
Voltage / V
Time / hour

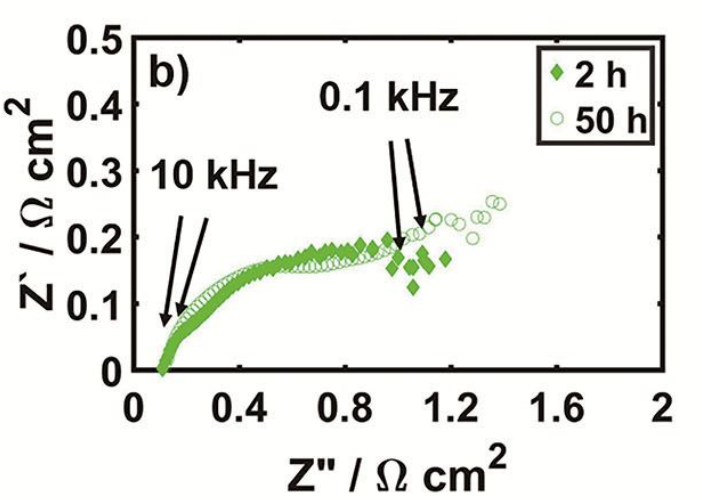
b)
2 h
50 h
0.1 kHz
10 kHz
Z` / Ω cm2
Z" / Ω cm2

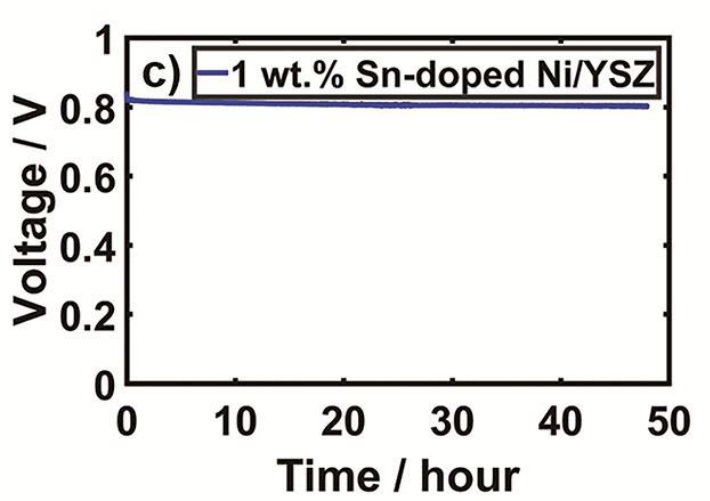
c)
1 wt.% Sn-doped Ni/YSZ
Voltage / V
Time / hour

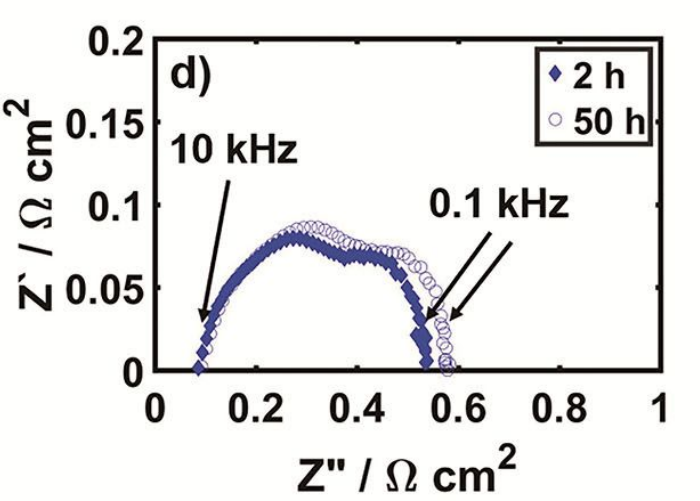
d)
2 h
50 h
10 kHz
0.1 kHz
Z` / Ω cm2
Z" / Ω cm2

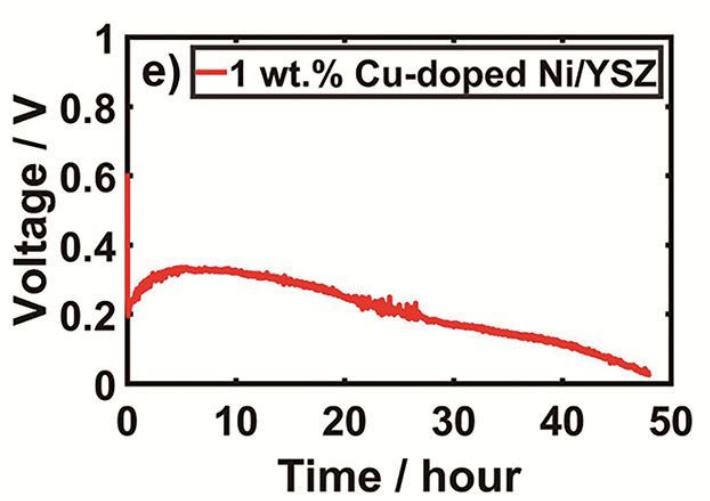
e)
1 wt.% Cu-doped Ni/YSZ
Voltage / V
Time / hour

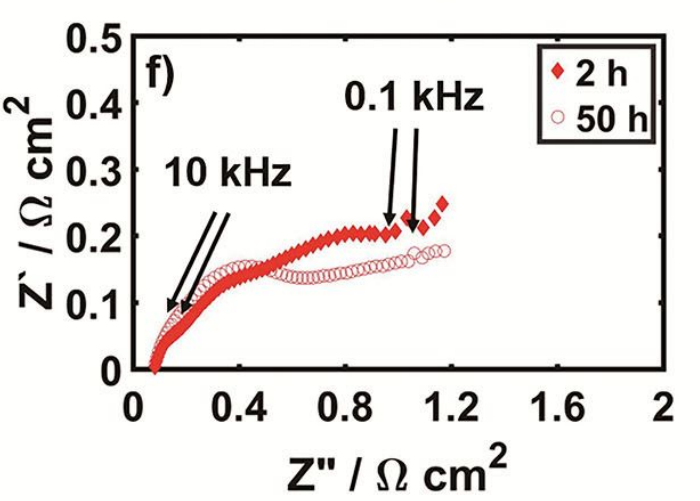
f)
2 h
50 h
0.1 kHz
10 kHz
Z` / Ω cm2
Z" / Ω cm2

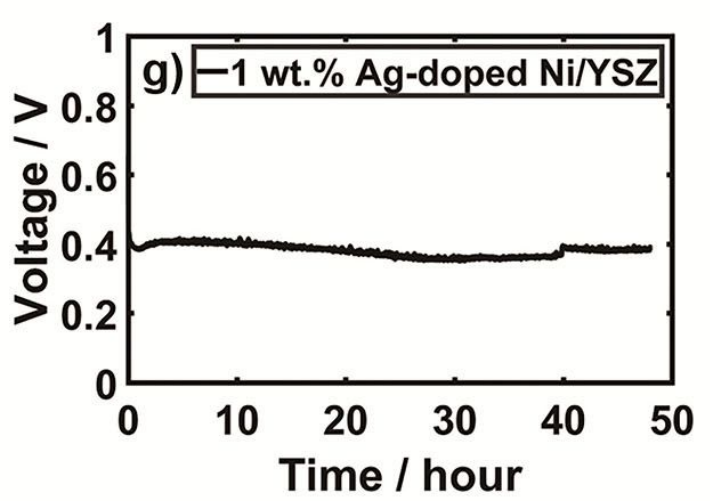
g)
1 wt.% Ag-doped Ni/YSZ
Voltage / V
Time / hour

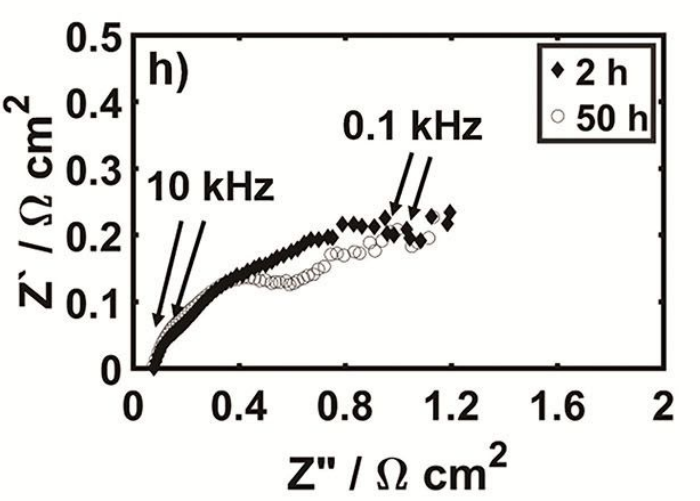
h)
2 h
50 h
0.1 kHz
10 kHz
Z` / Ω cm2
Z" / Ω cm2

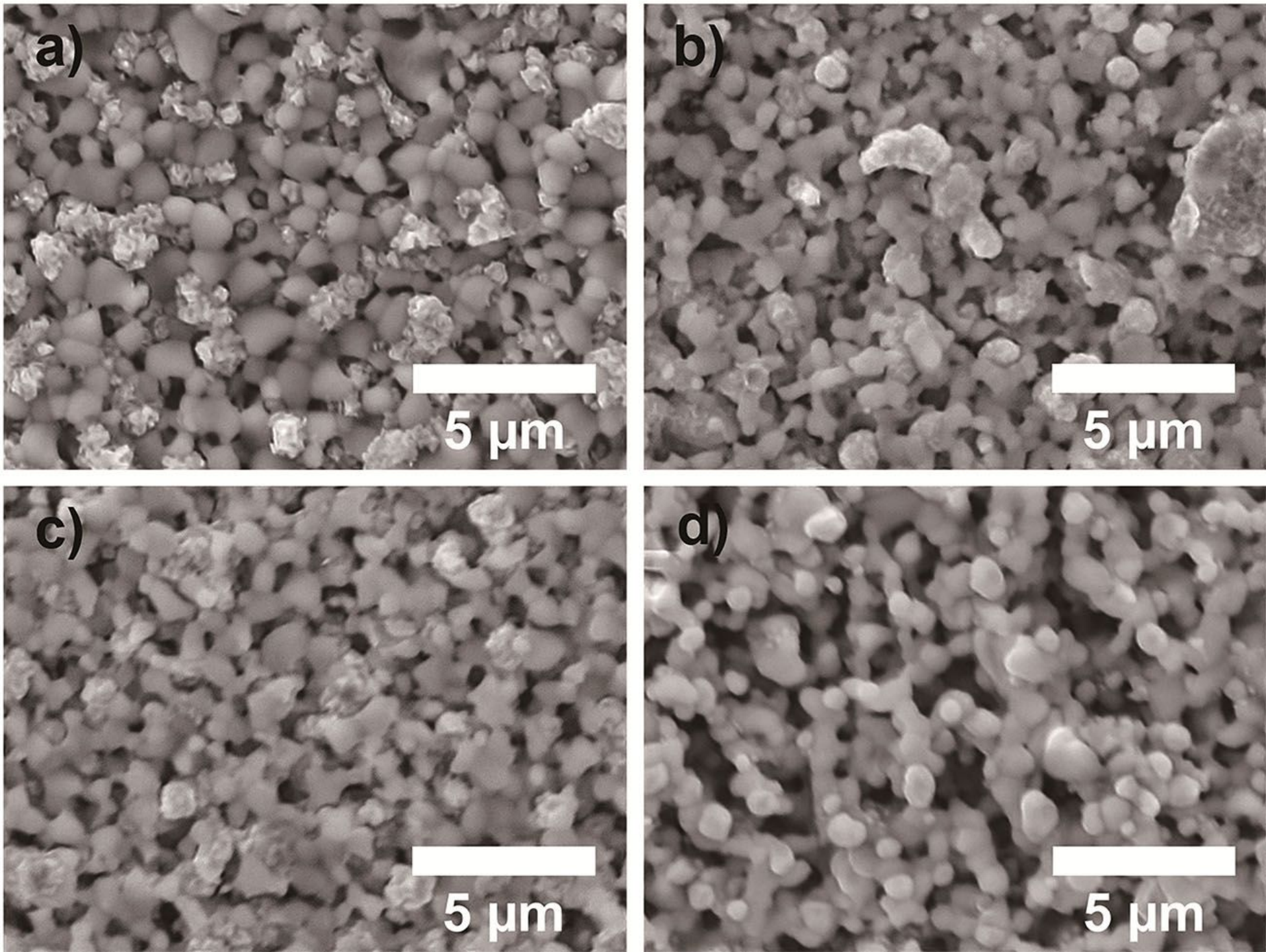
a)
5 µm
b)
5 µm
c)
5 µm
d)
5 µm